Research Article

SOHAG JOURNAL OF SCIENCES

https://doi.org/10.21608/sjsci.2023.236593.1124

The Interplay Between Heat Treatment and The Optical and Dielectric Properties of $Nd_{0.7}Ca_{0.3}MnO_3$

Sara A. Mohamed[1], Ibrahim Y. Khaled[1], I. A. Abdel-Latif[2], and Mahrous R. Ahmed[1,*]

[1] *Physics Department, Faculty of Science, Sohag University, Sohag 82524, Egypt*
[2] *Reactor Physics Department, Reactors Division, Nuclear Research Center, Egyptian Atomic Energy Authority, Cairo, Egypt*
**Email: mahrous.r.ahmed@science.sohag.edu.eg*

Received: 14th September 2023, **Revised:** 11th November 2023, **Accepted:** 12th November 2023
Published online: 24th December 2023

Abstract: In the current study, the influence of heat treatment on the structural, electrical, optical, and dielectric properties of $Nd_{0.7}Ca_{0.3}MnO_3$ compound has been examined. Heat treatment affects structural, electrical, optical, and dielectric properties. XRD results showed that the crystallinity decreased with increasing the annealing temperature. While the other crystal parameters increase. All samples have semiconductor behavior. Urbach energy has been investigated. The dispersion parameters are obtained using single-oscillator models.
Keywords: $Nd_{0.7}Ca_{0.3}MnO_3$, Manganite, Optical, dielectric properties, Urbach energy.

1. Introduction

Manganite materials are based on manganese oxide. They have the chemical formula $A_{1-x}R_xMnO_3$; where A = La, Pr, Nd and R = Sr, Ca, Ba. At T = TC (TC is the Curie temperature). These materials undergo a transition from ferromagnetic to paramagnetic, which occurs at finite "doping," $0< x < 0.25$, and is followed by a sharp rise in conductivity. One of these materials' most amazing fundamental properties is the ability to transfer from an insulating state to a metallic and magnetic one. Perovskite materials display a variety of fascinating characteristics, both in terms of theory and practical applications. Due to the enormous applications of these materials, many researches dealt with a detailed study of the properties of these materials [1-6].

Observed characteristics of this family include colossal magnetoresistance (CMR), ferroelectricity, superconductivity, charge ordering (CO), spin-dependent transport, high thermopower, and the interaction of structural, magnetic, and transport properties. These substances are suitable for memory devices and spintronics applications [7] as well as being employed as sensors and catalyst electrodes in some types of fuel cells. Numerous ceramic minerals, such as manganites, cobaltite's, and cuprates, have perovskite-like structures and frequently include three or more metals, such as manganese, cobalt, or copper, with certain oxygen slots left empty. The majority of the science that underlies as well as the basic physical characteristics of doped $LaMnO_3$, which is referred to as "manganites," were understood more than 40 years ago. The method provides a level of chemical flexibility that enables a systematic examination of the relationship between the oxides structure, electronic characteristics, and magnetic properties.

Over the past ten years, there has been a significant increase in the study of manganites and several phenomena, including the Jahn-Teller effect, double exchange contact [8], and enormous magnetoresistance. Since the discovery of colossal magnetoresistance (CMR) [8-11], which occurs when the application of a magnetic field of a few teslas causes an increase in conductivity of up to a few orders of magnitude in manganites, researchers have focused heavily on this material [9, 12-15].

Phase separation contributes to this phenomenon, which can take many different forms, including ferromagnetism, antiferromagnetism, charge order, and orbital order in manganites. Even while one phase typically predominates, numerous compatible phases (such as ferromagnetism and antiferromagnetism) can exist in the same crystal at the same time and be spatially separated from one another. Resonant elastic soft x-ray scattering, and light emission electron microscopy work together to reveal the forms of order present as well as the domain size. Soft x-rays are the perfect tool for measuring each phase separately.

In this study, we demonstrate how much the heat treatment affects the structural, electrical, dielectric and optical characteristics of $Nd_{0.7}Ca_{0.3}MnO_3$ samples that were made utilizing the solid-state reaction technique.

2. Materials and methods

Solid state reaction method was used to prepare the $Nd_{0.7}Ca_{0.3}MnO_3$. The preparation method was explained previously [16]. In the temperature range of 80-290K, the usual four-point approach was used to measure the temperature dependency of resistivity with and without magnetic field (0, 0.6 & 1.15 Tesla) using Oxford Instruments Limited (Oxford OX20DX). The optical properties were measured using a Jasco V-570 twin beam UV-visible-NIR spectrometer [17]. Utilizing LCR meters of the Hioki IM3536 type, the dielectric properties were studied. [18].

3. Results and Discussion:

3.1. Structure properties

XRD patterns for as prepared and annealed samples of $Nd_{0.7}Ca_{0.3}MnO_3$ (Tan= 700, 800 & 900°C) were plotted and discussed in previous work. Formula 1 is used to calculate the average crystallite size, which varied from 27.35 to 20.02nm depending on the annealing temperature, which ranged from 0 to 900°C. Additionally, the lattice micro-strain (ε_C) and dislocation density (δ) of all Nd-Ca-Mn-O peaks are determined, and their results are presented in Table 1 along their respective values see Figure 1.

The crystallite size of the sample is determined using Scherrer's formula [19]:

$$D = \frac{0.94\lambda}{\beta cos\theta}\ (nm) \quad (1)$$

where λ is the wavelength of incident XRD radiation (λ = 1.541838), β is the fullwidth at half maximum (FWHM) and θ is the Bragg's diffraction angle of the peak. The dislocation density is given by the following formula [20]:

$$\delta = \frac{1}{D^2}\ (nm)^{-2} \quad (2)$$

The number of crystallites per unit area is given by [21]:

$$N = \frac{t}{D^3}\ (nm)^2 \quad (3)$$

where t is the film thickness.

Microstrain, a form of lattice imperfection, is a distortion of the crystal lattice that results in a variation of the d-spacing within or between crystal domains [22].

$$\varepsilon_c = \frac{\beta \cos\theta}{4 \sin\theta} \quad (4)$$

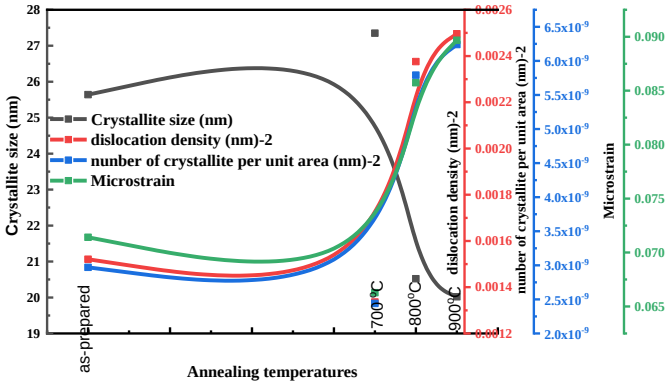

Fig.1: The crystallite parameters as a function of annealing temperature.

Table.1: The crystallite lattice parameters for as prepared and annealed Nd-Ca-Mn-O samples.

Sample	FWHM	Crystallite size (nm)	dislocation density $(nm)^{-2}$	number of crystallite per unit area $(nm)^{-2}$	Microstrain
Green	0.32	25.64	0.001521	2.97E-09	0.071414895
700	0.3	27.35	0.001336	2.44E-09	0.066280619
800	0.4	20.52	0.002376	5.79E-09	0.085737416
900	0.41	20.02	0.002496	6.24E-09	0.089674759

It is clear that the crystallite size decreases with increasing the annealing temperatures. While the dislocation density, the number of crystallites per unit area and the microstrain increase with increasing the annealing temperatures.

3.2. The electrical properties

Figure 2 shows the temperature dependence of the resistivity with and without magnetic field 0, 0.6 and 1.15 Tesla. For as prepared sample, see Fig.2(a), and the annealed sample at 700°C (see Fig.2(b)) show a semiconductor behavior. While annealed samples at 800 and 900°C without applied magnetic field show metal semiconductor behavior, see Fig.2(c) and (d). The value of Tms in zero magnetic is 105 and 110K respectively. With applied a magnetic field (0.6 and 1.15 T) the annealed samples show semiconductor behavior. For as prepared sample there is no change in the resistivity when a magnetic field is applied. The resistivity increases for applied magnetic field and then decrease see Fig.2(b) and (d), which due to aligned the spins with magnetic field. It can be seen from Figure.2(c) the resistivity decreases with applied the magnetic field.

3.3. Magnetoresistance

A change in the resistance caused by the applied magnetic field is known as magnetoresistance. Magnetoresistance is defined as:

$$MR = \frac{\rho(H)-\rho(0)}{\rho(0)}\% \quad (5)$$

Where $\rho(H)$ and $\rho(0)$ are the resistivity with and without magnetic field, respectively.

Figure 3 displays the magnetoresistance (MR) plots for as-prepared and annealed samples at various annealing temperatures (700, 800, and 900°C). The MR measurements show positive values. Increasing the annealing temperature, generally, results in an increase in all MR values. The annealed sample at 700°C has the highest value of MR near room temperature (MR%=2115%).

The positive high value of MR may be due to oxygen deficiency [23] and reduction in grain size [24]. For applied magnetic field 0.6T, all samples except the annealed sample at 700°C MR changed from positive to negative values. This could means that at H=0.6, where the applied magnetic field on the ferromagnetic domains causes them to align, the resistance drops because the magnetic field effect cancels out the effect of the annealing process on the localization of the magnetic states [16].

In Fig.3(a), MR of the annealed samples 700ºC and 900ºC, with applied magnetic field = 0.6 T, has the same behavior. These two samples have transition temperatures equal to 240ºC and 170ºC respectively. Where, MR of the as-prepared sample and the annealed sample at 800ºC with applied magnetic field 0.6 T has opposite behavior. However, in Fig.3(b), MR of the annealed samples at 700ºC and 900ºC with applied magnetic field 1.15 T still has the same behavior. These two samples have transition temperatures equal 210ºC and 160ºC respectively. The role of the applied magnetic field in the transition temperature is clear where the transition temperature decreases with increasing the applied magnetic field.

3.4. Optical properties

The transmittance T(λ)% and the reflectance R(λ)% of as prepared $Nd_{0.7}Ca_{0.3}MnO_3$ and annealed samples are measured in the spectral range (250–2500) nm. The optical characteristics of thin films can be analysed to obtain precise

information on their important and governing physical characteristics, which are necessary for the use of optical devices.

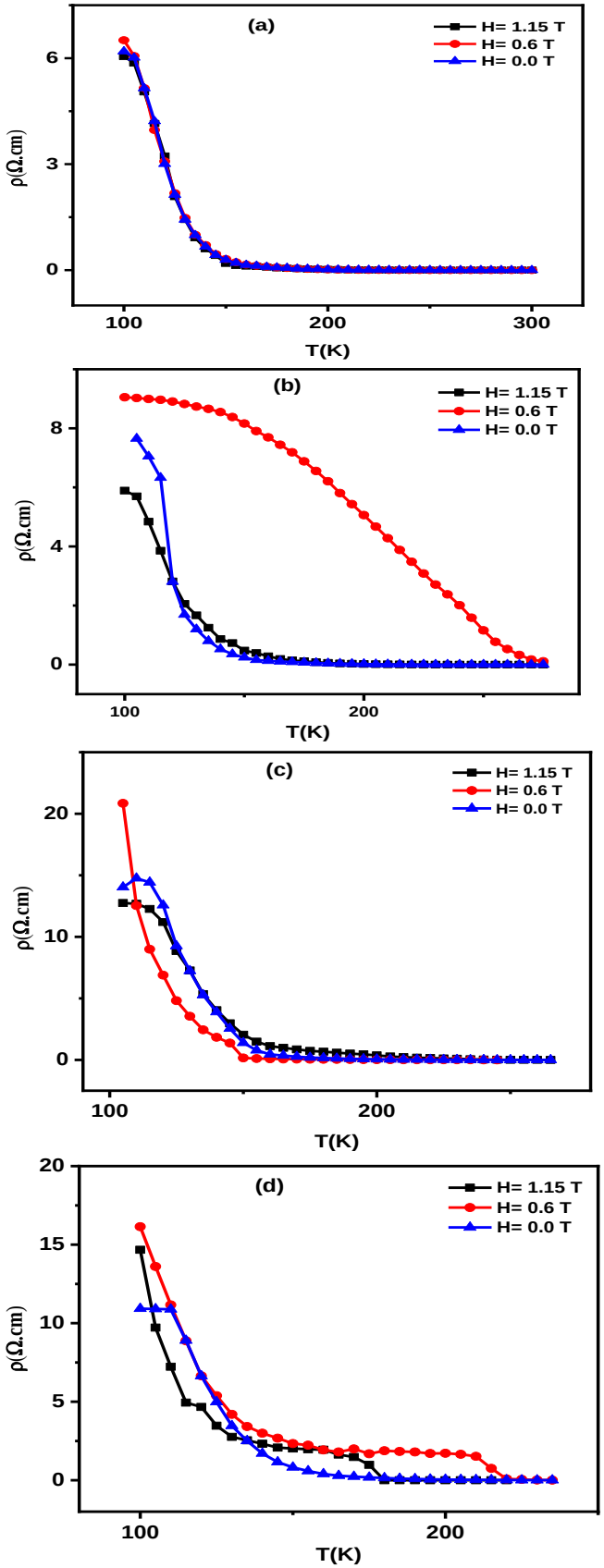

Fig.2: The variation of resistivity versus annealing temperatures.

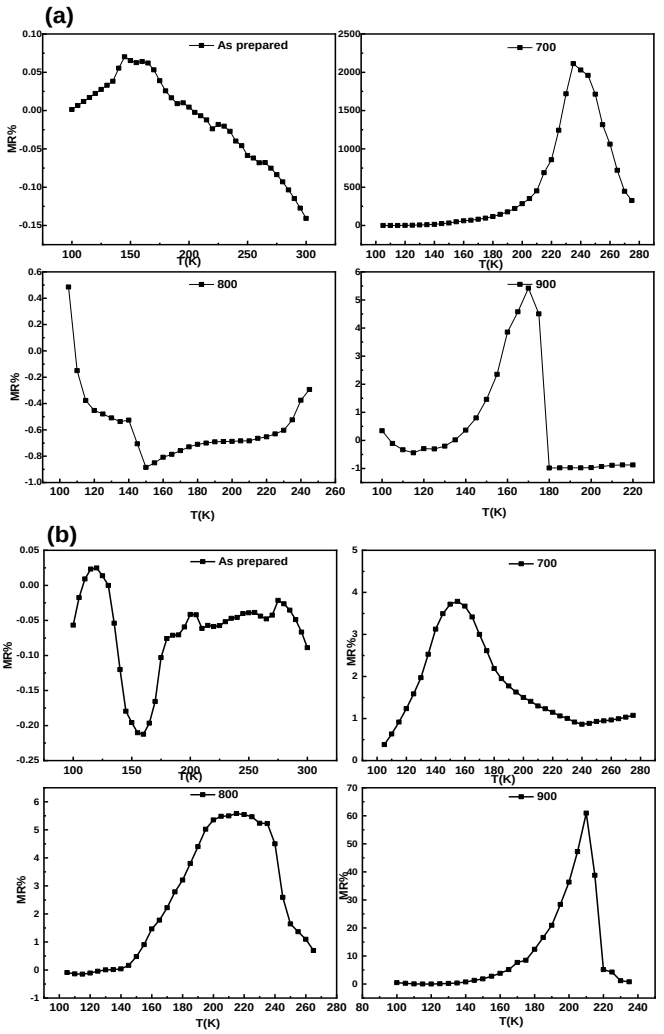

Fig.3: (a) The magnetoresistance versus temperature for applied magnetic field 0.6T (b) The magnetoresistance versus temperature for applied magnetic field 1.15 T.

These characteristics include the energy band gap, dispersion energy, oscillating energy, dielectric parameters, and linear and nonlinear parameters. The degree of disorder present in the amorphous and polycrystalline structure [25], in accordance with the Mott and Davis model [26], controls the width of localized states. The following Urbach equation can be used to determine Eu. Urbach tail is the width of localized state:

$$\alpha(h\nu) = \alpha_0 \, e^{h\nu/E_U} \quad (6)$$

where α_0 is a constant. Figure 4 shows the absorption coefficient, α, as a function of photon energy. It decreases exponentially with increasing the energy of the incident light. As shown in Fig.5, the slopes of the lines connecting ln (α) and photon energy E(eV) can be used to calculate the Urbach energy, E_U. By comparing the values of Urbach energy and energy gap, Eg, calculated in the previous research [16] (see Fig.6), the energy gap behaves oppositely to the Urbach energy according to the annealing temperatures. It is clear that with increasing the annealing temperatures the Urbach energy increases and then decreases, this refers to a decrease in the degree of disorder. Because of this, the band tail is reduced, and the band energy gap rises as a result.

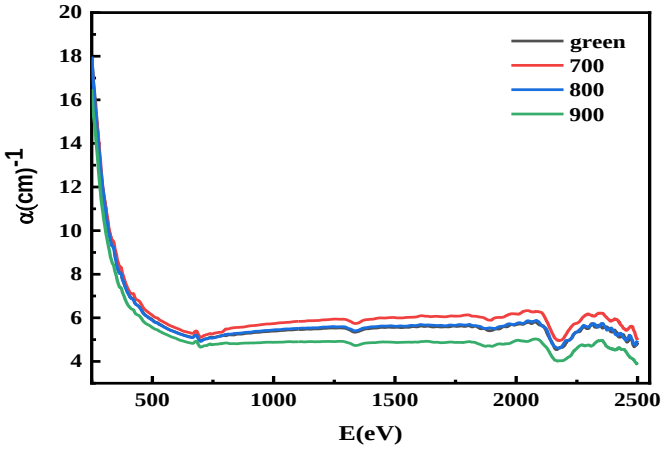

Fig.4: The absorption coefficient versus photon energy for as-prepared and annealed samples.

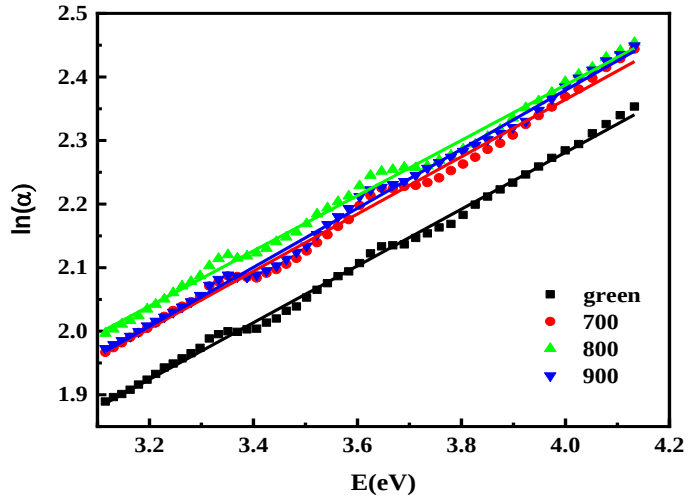

Fig.5: ln(α) versus photon energy for as prepared and annealed samples.

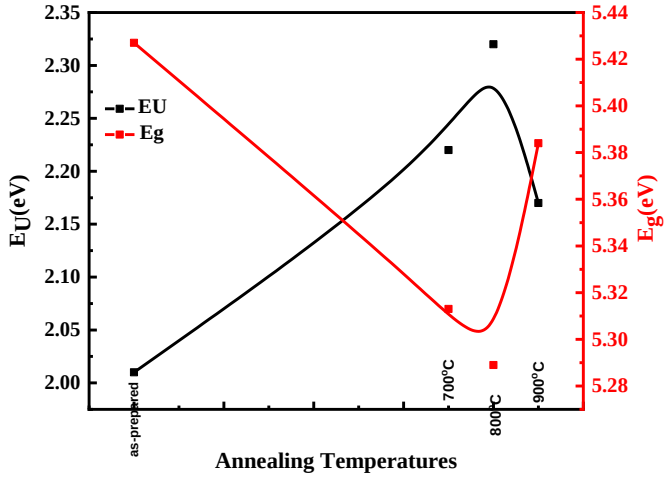

Fig.6: Urbach energy and energy gap versus annealing temperatures for as prepared and annealing temperatures.

Dispersion characteristics have a major role in the design of devices used in optical communications and other opto-electronics. The dispersion spectra in the transparent region λ >700 nm were studied according to Wemple and DiDomenico model [27, 28]. The dispersion energy E_d, and the single oscillator energy, E_o, can be calculated by the following relation:

$$(n^2-1)^{-1} = \frac{E_0}{E_d} - \frac{(h\nu)^2}{E_0 E_d} \qquad (7)$$

By plotting $(n^2\text{-}1)^{-1}$ versus $(h\nu)^2$ as seen in Figure 7, E_o and E_d are calculated for as prepared and annealed samples by using the slope and intercept on the vertical axis (see inset Figure). For as prepared sample E_o and E_d are 4.9 eV and 1.7 eV respectively. With increasing the annealing temperatures, the values of E_o and E_d increase see Fig.8. This change suggests that the annealing temperatures causes material disorder that increases with increasing the annealing temperatures value.

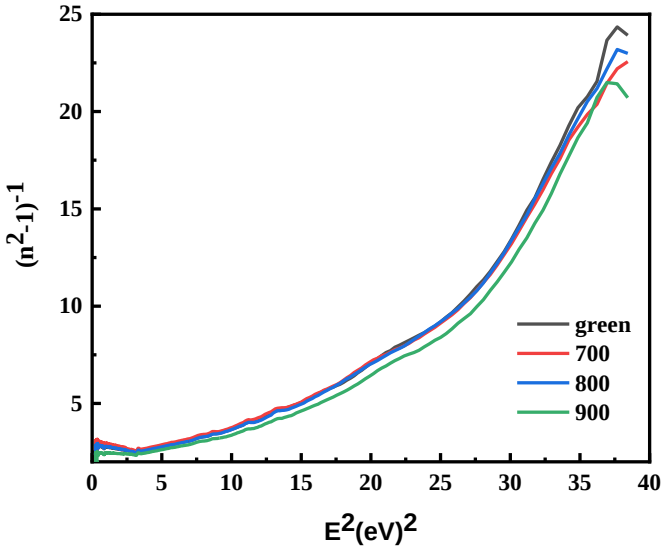

Fig.7: $(n^2\text{-}1)^{-1}$ versus E^2 for as prepared and annealing samples.

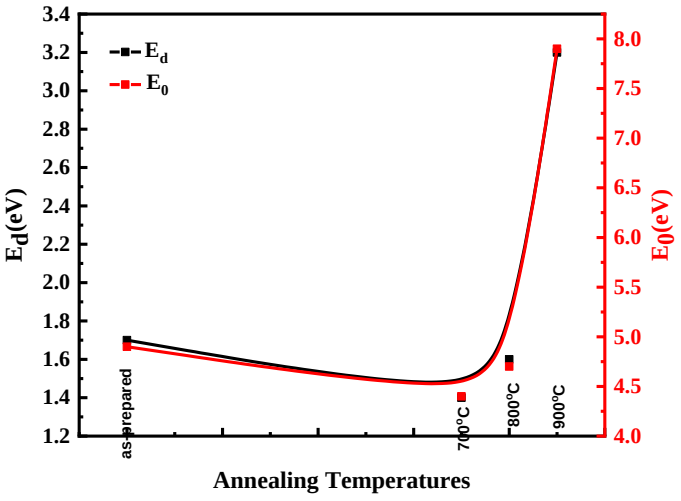

Fig.8 The oscillator energy and the oscillator strength versus annealing temperature for as prepared and annealed samples.

3.5. Dielectric Properties

Dielectric materials have molecules that align with an electric field when the AC field is applied to the material. Each molecular moment produced by this alignment has an electric dipole. When the molecules electric dipole moments interact, an electric field that is in opposition to the applied field is

produced [29-32]. As depicted in the Figure 9, there is an inverse relationship between the imaginary part of the impedance, Z'', and the real part in a dielectric material. This can be attributed to the polarization behavior of dielectrics when it is subjected to an electric field.

The strength of the opposing electric field depends on the frequency of the applied field. At low frequencies, the molecules have time to align themselves with the applied field, and the opposing electric field is strong. At high frequencies, the molecules do not have time to align themselves with the applied field, and the opposing electric field is weak [33-35] When considering the impedance, which comprises both the imaginary and real parts, we can observe that the imaginary part reflects the magnitude of the opposing electric field, while the real part indicates the level of polarization exhibited by the dielectric material. Consequently, at lower frequencies, the imaginary part of the impedance tends to be significant, accompanied by a relatively small real part. This phenomenon can be attributed to the strength of the opposing electric field being higher and the polarization of the dielectric material being comparatively lower. In contrast, the real component of the impedance is big and the imaginary part is tiny at high frequencies. This is due to the weak opposing electric field and high degree of polarization in the dielectric substance. The distinct behavior of the annealed sample at T_{an}=800 ^{0}C is caused by the existence of multiple relaxation phases or non-linear behaviors, suggesting the relaxation phenomena to be of the non-Debye type[36, 37].

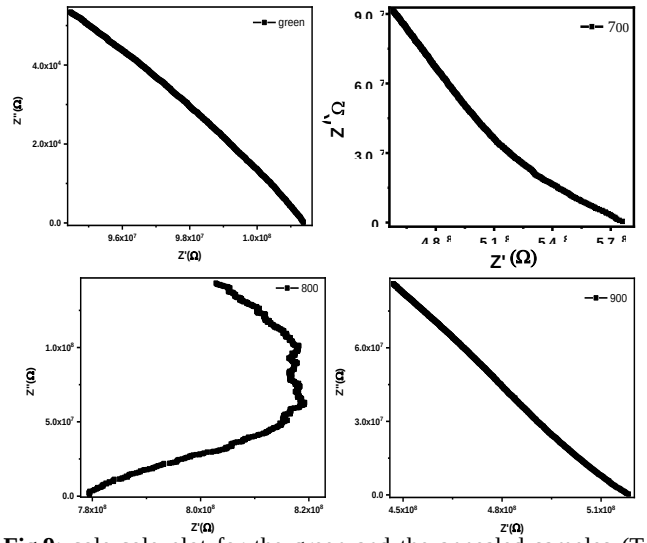

Fig.9: cole-cole plot for the green and the annealed samples (T_{an} = 700, 800 and 900°C) for $Nd_{0.7}Ca_{0.3}MnO_3$.

4. Conclusion

The investigation results of structural and some physical properties of as-prepared sample of $Nd_{0.7}Ca_{0.3}MnO_3$ annealed at 700°C, 800°C and 900°C samples are concluded as following:

The crystallinity decreased with increasing the annealing temperature. While the other crystal parameters increased. All samples had semiconductor behavior. Urbach energy was investigated. The dispersion parameters were obtained using single-oscillator models.

CRediT authorship contribution statement:

I. A. Abdel-Latif proposed the concept of the paper. Ibrahim Y. Khaled and Sara A. Mohamed were responsible for designing and executing the experimental setup. They conducted experimental measurements. Mahrous R. Ahmed performed the necessary revisions to the manuscript.

Data availability statement

The data used to support the findings of this study are available from the corresponding author upon request.

Declaration of competing interest

The authors declare that they have no known competing financial interests or personal relationships that could have appeared to influence the work reported in this paper.

Acknowledgments

The authors gratefully thank Sohag University for supporting this work. The authors are grateful for grant No 45643 from STDF.

References

[1] A. Ahmed, H. Mohamed, J. Paixão., S. A. Mohamed, *Journal of Magnetism and Magnetic Materials*, 456 (2018) 217-222.
[2] A. Ahmed, H. Mohamed, A. Diab, S. A. Mohamed, *Indian Journal of Physics*, 91 (2017) 169-181.
[3] A. Ahmed, H. Mohamed, A. Diab, S. A. Mohamed, S. García-Granda, Martínez-Blanco D, *Solid State Sciences*, 57 (2016) 1-8.
[4] H. Mohamed, M. Ahmed, M. R. Ahmed, J. Paixão, S. Mohamed, *physica status solidi (b)*, 260 (2023) 2300175.
[5] A. Ahmed, M. R. Ahmed, A. Saad, *Journal of Electromagnetic Analysis and Applications*, 3 (2011) 27.
[6] M. R. Ahmed, *Journal of Magnetism and Magnetic Materials*, 504 (2020) 166628.
[7] J. Coey, M. Viret, S. Von Molnar, *Advances in physics*, 48 (1999) 167-293.
[8] C. Zener, *Physical Review*, 82 (1951) 403.
[9] R. Von Helmolt, J. Wecker, B. Holzapfel, I. Schultz, K. Samwer, *Physical Review Letters*,71 (1993) 2331.
[10] G. Jonker, J. Van Santen, *physica*, 16 (1950) 337-349.
[11] E. Wollan, W. Koehler, *Physical Review*, 100 (1955) 545.
[12] M. R. Kusters, J. Singleton, D. Keen, R. McGreevy, W. Hayes, *Physica B: Condensed Matter*, 155 (1989) 362-365.
[13] S. Okayasu, K. Miyabe, K. Chahara, A. Tominaga, Y Narahara, *Solid state communications*, 73 (1990) 593-6.
[14] S. Jin, H. T. Tiefel, M. McCormack, R. Fastnacht, R. Ramesh, L. Chen, *Science*, 264 (1994) 413-5.
[15] Y. Tomioka, A. Asamitsu, H. Kuwahara, Y. Moritomo, Y. Tokura, *Physical Review B*, 53 (1996) R1689.
[16] S. A. Mohamed, I. Abdel-Latif, I. Y. Khaled, M. R. Ahmed, *Information Sciences Letters*, 12 (2023) 2521-2537.
[17] S. A. Mohamed, M. R. Ahmed, H. Ali, A. A. Hakeem, *Physica Scripta*, 97 (2022) 045810.
[18] A. A. Hakeem, E. Ibrahim, H. Ali, M. Abd El-Raheem, A. Hamazaoui, M. R. Ahmed, *Physica Scripta*, 97 (2022) 025803.
[19] A. Patterson, *Physical review*, 56 (1939) 978.
[20] P Gay, P. Hirsch, A. Kelly, *Acta metallurgica*, 1 (1953) 315-9.
[21] T. W. Read, W. Shockley, *Physical review*, 78 (1950) 275.
[22] H. Jiang, M. Rühle, E. Lavernia, *Journal of materials research*, 14 (1999) 549-59.

[23] H. L. Ju, J. Gopalakrishnan, J. Peng, Q. Li, G. Xiong, T. Venkatesan, L. R. Greene, *Physical Review B*, 51 (1995) 6143.
[24] J. A. Millis, B. P Littlewood, I. B. Shraiman, *Physical review letters*, 74 (1995) 5144.
[25] D. Singh, S. Kumar, R. Thangaraj, *Phase Transitions*, 87 (2014) 206-222.
[26] A. Atta, M. El-Nahass, M. K. Elsabawy, M. Abd El-Raheem, A. Hassanien, A. Alhuthali, *Pramana*, 87 (2016) 1-8.
[27] S. Wemple, M. Jr. DiDomenico, *Physical Review B*, 3 (1971) 1338.
[28] S. Wemple, *Physical Review B*, 7 (1973) 3767.
[29] W. P. Atkins, S. R. Friedman, Molecular quantum mechanics. Oxford university press, Oxford, 2011.
[30] H. G. Haertling, *Journal of the American Ceramic Society*, 82 (1999) 797-818.
[31] H. Fröhlich, *Proceedings of the National Academy of Sciences*, 72 (1975) 4211-4215.
[32] P. R. Twitchell, E. Carr, *The Journal of Chemical Physics*, 46 (1967) 2765-2768.
[33] Moya X, Kar-Narayan S, Mathur ND, *Nature materials*, 13 (2014) 439-450.
[34] M. J. Jin, Theory and computation of electromagnetic fields: John Wiley & Sons, New York, 2015.
[35] X. Huang, B. Sun, Y. Zhu, S. Li, P. Jiang, *Progress in Materials Science*, 100 (2019) 187-225.
[36] K. S. Barik, M. Panda, M. K. Prasad, S. Sahoo, R. Choudhary, *Circuits and Systems*, 2 (2022) 100013.
[37] K. Yadagiri, R. Nithya, *Journal of Physics and Chemistry of Solids*, 158 (2021) 110232.